A&A 612, A83 (2018)
https://doi.org/10.1051/0004-6361/201732355

Astronomy & Astrophysics

Formation of interstellar methanol ice prior to the heavy CO freeze-out stage

D. Qasim[1], K.-J. Chuang[1], G. Fedoseev[2], S. Ioppolo[3,4], A. C. A. Boogert[5], and H. Linnartz[1]

[1] Sackler Laboratory for Astrophysics, Leiden Observatory, Leiden University, PO Box 9513, 2300 RA Leiden, The Netherlands
e-mail: dqasim@strw.leidenuniv.nl
[2] INAF–Osservatorio Astrofisico di Catania, via Santa Sofia 78, 95123 Catania, Italy
[3] School of Electronic Engineering and Computer Science, Queen Mary University of London, Mile End Road, London E1 4NS, UK
[4] School of Physical Sciences, STEM, Open University, Milton Keynes MK7 6AA, UK
[5] Institute for Astronomy, University of Hawaii at Manoa, 2680 Woodlawn Drive, Honolulu 96822-1839, USA

Received 24 November 2017 / Accepted 17 January 2018

ABSTRACT

Context. The formation of methanol (CH_3OH) on icy grain mantles during the star formation cycle is mainly associated with the CO freeze-out stage. Yet there are reasons to believe that CH_3OH also can form at an earlier period of interstellar ice evolution in CO-poor and H_2O-rich ices.
Aims. This work focuses on CH_3OH formation in a H_2O-rich interstellar ice environment following the OH-mediated H-abstraction in the reaction, CH_4 + OH. Experimental conditions are systematically varied to constrain the CH_3OH formation yield at astronomically relevant temperatures.
Methods. CH_4, O_2, and hydrogen atoms are co–deposited in an ultrahigh vacuum chamber at 10–20 K. OH radicals are generated by the H + O_2 surface reaction. Temperature programmed desorption – quadrupole mass spectrometry (TPD–QMS) is used to characterize CH_3OH formation, and is complemented with reflection absorption infrared spectroscopy (RAIRS) for CH_3OH characterization and quantitation.
Results. CH_3OH formation is shown to be possible by the sequential surface reaction chain, $CH_4 + OH \rightarrow CH_3 + H_2O$ and $CH_3 + OH \rightarrow CH_3OH$ at 10–20 K. This reaction is enhanced by tunneling, as noted in a recent theoretical investigation Lamberts et al. (2017, A&A, 599, A132). The CH_3OH formation yield via the CH_4 + OH route versus the CO + H route is approximately 20 times smaller for the laboratory settings studied. The astronomical relevance of the new formation channel investigated here is discussed.

Key words. astrochemistry

1. Introduction

Methanol (CH_3OH) is an important interstellar molecule. CH_3OH has been observed abundantly in both the gas phase (Friberg et al. 1988; Turner 1998; Parise et al. 2002; Bergman et al. 2011; Wirström et al. 2011; Guzmán et al. 2013; Öberg et al. 2014; Taquet et al. 2015) and the solid state (Grim et al. 1991; Allamandola et al. 1992; Skinner et al. 1992; Chiar et al. 1996; Dartois et al. 1999; Gibb et al. 2000, 2004; Pontoppidan et al. 2003; Taban et al. 2003; Boogert et al. 2008, 2011; Bottinelli et al. 2010). It is generally accepted that CH_3OH formation is most efficient by solid state interactions on icy grain mantles. Models, supported by experiments, of gas phase synthesis of CH_3OH provide abundances orders of magnitude below the observed fractional abundance of CH_3OH (Garrod et al. 2006; Geppert et al. 2006), while solid state laboratory studies show that CH_3OH is efficiently formed in CO-rich ices through sequential hydrogenation of CO (Hiraoka et al. 1994; Watanabe & Kouchi 2002; Fuchs et al. 2009). This is further supported by computational models (Cuppen et al. 2009; Fuchs et al. 2009; Garrod et al. 2006) that show that hydrogenation of CO ice leads to the production of CH_3OH. Indeed, these findings are in line with the spectroscopic interpretation of observational data; CO and CH_3OH are found to coexist in CO-rich and H_2O-poor interstellar ices (Cuppen et al. 2011; Boogert et al. 2015; Penteado et al. 2015). Not only is it a prevalent interstellar molecule, but CH_3OH is also an important precursor in the formation of larger species. Öberg et al. (2009) illustrated that upon vacuum UV irradiation, CH_3OH can break apart into fragments that can recombine to form complex organic molecules (COMs). In UV-rich environments in the interstellar medium, the formation of CH_3OH may thus be crucial to the formation of larger COMs. The studies by Chuang et al. (2015, 2017) and Fedoseev et al. (2017) show that CH_3OH may be a key player in the formation of larger COMs, also for cold dense prestellar core conditions. The authors show that radicals derived from CH_3OH via an abstraction process can recombine or combine with other radicals, resulting in the formation of COMs as large as glycerol, even at temperatures below 20 K and without the need for UV-induced radiation.

Recent theoretical and experimental efforts (Lamberts et al. 2017) have provided results that have sparked the idea of H_2O and CH_3OH coexisting in a CO-poor and H_2O-rich inter stellar ice. Such ices are thought to form before the "heavy" CO freeze out stage, which starts to occur at a cloud extinction (A_V) of $A_V > 3$ and dust temperatures <20 K, and that is followed by the "catastrophic" CO freeze-out stage at $A_V > 9$ and dust temperatures also <20 K. Prior to the heavy CO freeze-out stage,

a CO:H_2O ice ratio of <5% is expected due to some CO freezing out as well as atom-addition reactions (C, O, H, etc.). Due to the relatively low gas densities at this stage, only a relatively low amount of CO is able to accrete onto dust grains, as examined in Pontoppidan (2006) and discussed in Öberg et al. (2011), Boogert et al. (2015), and van Dishoeck (2017). This time period is known as the "H_2O-rich ice phase" or "polar ice phase" (i.e., the phase that lacks CO ice). CH_3OH formation through this reaction, CH_4 + OH, can take place in this phase. However, this does not exclude this reaction to also take place during the CO freeze-out stage, where CH_3OH formation is normally dominated by CO hydrogenation. During this time, O_2 might be intimately mixed with CO (Vandenbussche et al. 1999) and can be hydrogenated to form OH radicals. Gas phase CH_4 becomes more dominant relative to atomic carbon (van Dishoeck 1998) and could freeze out with CO. The importance of the present study is that it focuses on a phase in which CH_3OH is only formed through CH_4 + OH, as CO is not frozen out yet, and an identification of CH_3OH in corresponding environments, therefore, directly relates to this alternative reaction pathway.

The study by Lamberts et al. (2017) was done to provide reaction rates at cryogenic temperatures of the reaction between methane (CH_4) and OH as CH_4 has been observed in the H_2O-rich ice phase (Boogert et al. 1997; Öberg et al. 2008), and OH radicals are expected to be abundant in that phase (Cuppen & Herbst 2007; Ioppolo et al. 2008; Cuppen et al. 2010; Oba et al. 2012; Lamberts et al. 2013). These authors, as well as others (Wada et al. 2006; Hodyss et al. 2009; Weber et al. 2009; Zins et al. 2012; Bossa et al. 2015), showed that CH_4 hydrogen abstraction by an OH radical results in the efficient formation of CH_3 radicals; a process that can be induced by tunneling (Lamberts et al. 2017). Thus, these findings can be taken one step further by postulation that the OH-induced abstraction reaction of CH_4 may result in the formation of CH_3OH by the sequential reaction chains: $CH_4 + OH \rightarrow CH_3 + H_2O$ and $CH_3 + OH \rightarrow CH_3OH$. There are already a number of laboratory experiments that exhibit CH_3OH formation via energetic processing of ice mixtures containing CH_4 and H_2O (Schutte 1988; d'Hendecourt et al. 1996; Moore & Hudson 1998; Wada et al. 2006; Hodyss et al. 2009; Martín-Doménech et al. 2016). In addition, Bergner et al. (2017) have explored the formation of CH_3OH via O-atom insertion in CH_4 molecules upon photo dissociation of O_2 in binary mixtures. In our paper, the reaction CH_4 + OH leading to the formation of CH_3OH under relevant cold dense core conditions is discussed. The OH radicals are already present at the earliest stages of ice formation via photo dissociation of H_2O molecules and by atomic H- and O-rich accreting gas (see, e.g., Boogert et al. 2015). Therefore, this formation mechanism could work even under non-energetic conditions, and can be extended to the formation of COMs that contain the hydroxyl functional group (–OH). Furthermore, CH_3 radical formation is constrained to abstraction reactions only, whereas in the energetic processing studies, it is unclear whether CH_3 radicals are formed by energetic and/or non-energetic pathways.

Data from astronomical observations also provide an incentive to explore CH_3OH ice formation before the heavy CO freeze-out stage (i.e., in the H_2O-rich ice phase). In the review published by Boogert et al. (2015), Fig. 7 displays the observed ice column densities of CH_3OH and H_2O, as well as other species, as a function of (A_V). Consistent with the current model of interstellar ice evolution, H_2O is concentrated at a lower A_V with respect to CH_3OH. However, taking a closer look at the figure reveals that CH_3OH upper limit values can be found at a lower A_V and at lower column densities than CH_3OH detections. Such upper limits do not prove that CH_3OH can be formed at lower A_V, but they also do not exclude the idea. A possible explanation for the relatively low A_V and column densities for the CH_3OH upper limits may be due to other reaction pathways expected to take place before the CO freeze-out phase. It is also possible that at such low A_V, the sensitivity of the telescopes used may not have been high enough. In the dawn of the *James Webb* Space Telescope (JWST) era, it is expected that soon it will be possible to extend on the formation schemes in which solid CH_3OH is formed or consumed.

In this paper, the formation of CH_3OH ice by CH_4 + OH under relevant cold dense core conditions is discussed. Section 2 provides an overview of the experimental conditions and methods. Section 3 details how CH_3OH was identified, formed in the ice, and quantified. Section 4 provides insights into how the laboratory results presented here can be used to constrain the ice chemistry in the H_2O-rich ice phase of cold prestellar core environments, as well as a discussion of Fig. 7 from Boogert et al. (2015). Section 5 summarizes the findings from this paper.

2. Experimental setup and methods

The experiments described here are performed with SURFRESIDE^2. This is a double atom beam line, ultrahigh vacuum (UHV) setup with a base pressure of $\sim 10^{-10}$ mbar in the main chamber. An in-depth description of the setup and experimental procedures can be found in Ioppolo et al. (2013) and Linnartz et al. (2015). Ices are grown on a gold-plated copper substrate (2.5×2.5 cm^2) that is attached to the cold-finger of a closed-cycle helium cooled cryostat (ColdEdge CH–204 SF). Temperatures as low as 7 K can be realized. The temperature settings are controlled by a LakeShore 340 temperature controller. The substrate temperature is measured by a silicon diode sensor (DT–670) with an absolute accuracy of 1 K. The substrate temperature is changed by resistive heating of a tungsten filament. Incorporation of a sapphire rod within the cryocooler allows substrate temperatures as high as 450 K.

The processes taking place in the ice can be studied through infrared (IR) spectroscopy and mass spectrometry. Species formed in the ice are probed by their IR signatures with a Fourier transform infrared spectrometer (FTIR; Agilent Cary 640/660) applying the reflection absorption infrared spectroscopy (RAIRS) technique. The FTIR permits a coverage of 6000–700 cm^{-1} with a resolution of 1 cm^{-1}. To further constrain species present in the ice, a quadrupole mass spectrometer (QMS; Spectra Microvision Plus LM76) is used to measure the desorption temperature of ice species during a temperature programmed desorption (TPD) run, as well as the mass spectrum of the desorbing species upon electron impact ionization. A commonly used electron impact ionization energy of 70 eV is chosen. All TPD experiments involve a linear ramp rate of 2 K min^{-1}.

In order to simulate cold dense core conditions, all ices are grown on a substrate surface with a temperature between 10–20 K. CH_4, H, and O_2 are admitted into the main vacuum chamber following the co deposition technique (i.e., different molecular species deposited simultaneously), which reproduces interstellar conditions better than with previously used predeposition techniques (i.e., different molecular species deposited sequentially; Linnartz et al. 2015). Additionally, this technique allows all deposited species to react with one another, regardless of the ice thickness, which is advantageous when trying to probe trace species. The OH radicals are formed by H-atom addition to O_2 (Cuppen et al. 2010) and the CH_3 radicals are formed by

Table 1. Experiments performed in this study.

No.	Experiments	Ratio CH_4:H:O_2	T_{sample}[a] (K)	$Flux_{CH_4}$ $cm^{-2}\,s^{-1}$	$Flux_H$ $cm^{-2}\,s^{-1}$	$Flux_{O_2}$ $cm^{-2}\,s^{-1}$	$Flux_{CH_3OH}$ $cm^{-2}\,s^{-1}$	$Flux_{H_2O}$ $cm^{-2}\,s^{-1}$	$Flux_{CO}$ $cm^{-2}\,s^{-1}$	Time (s)
1.0	$CH_4 + H + O_2$	1:2:1	10	3E12	6E12	4E12	–	–	–	43 200
2.0	$CH_4 + H + O_2$	1:2:1	10	3E12	6E12	4E12	–	–	–	21 600
2.1	$^{13}CH_4 + H + O_2$	1:2:1	10	3E12	6E12	4E12	–	–	–	21 600
2.2	$CH_4 + H + {}^{18}O_2$	1:2:1	10	3E12	6E12	4E12	–	–	–	21 600
2.3	$^{13}CH_4 + H + {}^{18}O_2$	1:2:1	10	3E12	6E12	4E12	–	–	–	21 600
3.0	CH_3OH	–	10	–	–	–	4E13	–	–	100
4.0	CH_3OH	–	10	–	–	–	1E13	–	–	1200
4.1	$CH_3OH + O_2$ (MWAS)[b]	–	10	–	–	4E13	1E11	–	–	9000
4.2	$CH_3OH + CH_4$	–	10	6E13	–	–	1E11	–	–	9000
4.3	$CH_3OH + H_2O$	–	10	–	–	–	1E11	6E13	–	9000
4.4	$CH_3OH + H_2O$ (MWAS)[b]	–	10	–	–	–	1E11	6E13	–	9000
4.5	$CH_3OH + H_2O$ (MWAS)[b] + CH_4	–	10	6E13	–	–	1E11	6E13	–	9000
4.6	$CH_3OH + CO$	–	15	–	–	–	2E10	–	7E10	3600
5.0	$^{13}CH_4 + H + {}^{18}O_2$	1:2:1[c]	20	3E12[c]	6E12	4E12	–	–	–	21 600
6.0	$CH_4 + H + O_2$	1:2:1	10	3E12	6E12	1E13	–	–	–	21 600

Notes. All fluxes, except the H flux, are derived from the Hertz–Knudsen equation. [a] Temperature of the sample at which the ices are grown. [b] The CH_4 flux is lower than the listed value in order to have the same CH_4:H_2O ice ratio as found in exp. 2.0. Thus, a constant CH_4 flux is not carried out in this particular experiment. [c] "(MWAS)" denotes species that were placed in the MWAS chamber. See also Sect. 3.2.

OH-mediated H-abstraction of CH_4 (i.e., radicals are formed in situ). A series of control experiments performed by Lamberts et al. (2017) showed that the produced OH radicals are solely responsible for the H-abstraction of CH_4 (i.e., formation of CH_3 radicals directly through reaction with H atoms is not efficient, as proved in Lamberts et al. (2017)). We note that the formation of OH radicals from O_2 is not necessarily representative of the formation of OH radicals in low A_V (low density) environments, where the O + H route dominates, as well as photodissociation of H_2O. Since the OH and CH_3 radicals are formed in the ice, they are expected to be thermalized before further reactions occur.

To perform H-atom addition reactions, H-atoms are produced by a hydrogen atom beam source (HABS; Tschersich & Von Bonin 1998; Tschersich 2000; Tschersich et al. 2008), and the H-atom beam line has an angle of 45° to surface normal of the gold-plated sample. Hydrogen molecules (H_2; Praxair 99.8%) flow into the HABS chamber via a leak valve and are thermally cracked by a tungsten filament. The gas deposition lines of O_2 (Linde Gas 99.999%) and CH_4 (Linde Gas 99.995%) are angled at 135° and 68°, respectively, to the plane of the sample's surface. Gas isotopologues, $^{18}O_2$ (Campro Scientific 97%) and $^{13}CH_4$ (Sigma-Aldrich 99%), are used as controls to aid in identification of the formed ice products.

Fluxes and column densities are characterized as follows. An absolute D-atom flux was measured by Ioppolo et al. (2013), and the O_2 and CH_4 fluxes are calculated using the Hertz–Knudsen equation (Kolasinski 2012). Column densities are determined by the relation between absorbance and column density, as described in Hudgins et al. (1993). As discussed previously by Ioppolo et al. (2013), Teolis et al. (2007), and Loeffler et al. (2006), such measurements must be done with caution. Therefore in this work, only the relative column densities of CH_4, H_2O, and CH_3OH are given (i.e., absolute column densities are not listed). Care is taken to use integrated absorbances that do not deviate from the linear trend of the column density over time. The band strength used to determine the CH_3OH column density is 7.1×10^{-17} cm molecule^{-1} (1030 cm^{-1}) and is obtained by performance of a He–Ne laser interference experiment in SURFRESIDE^2 (Chuang et al. in prep.,). The underlying experimental procedure is described in detail in Paardekooper et al. (2016). CH_4 (1302 cm^{-1}) and H_2O (1659 cm^{-1}) band strengths of 8.0×10^{-18} cm molecule^{-1} and 9.0×10^{-18} cm molecule^{-1}, respectively, are extracted from Bouilloud et al. (2015). Since the band strengths from Bouilloud et al. (2015) are obtained from transmission IR experiments, a proportionality factor between the CH_3OH band strengths from Bouilloud et al. (2015) and our laser interference experiment is used as a correction factor. It should be noted that literature transmission band strength values cannot be used with optical depth values obtained from a RAIRS experiment partly due to surface-enhanced dipole coupling that occurs in RAIRS. Setup specific values have to be determined for specified conditions. All experiments discussed in this paper are listed in Table 1.

3. Results and discussion

3.1. Identification and analysis of CH_3OH formation

In the next sections, three different ways to confirm the formation of CH_3OH ice by the reaction, CH_4 + OH, are presented.

3.1.1. TPD

Figure 1 (top) shows the TPD spectra of pure CH_3OH compared to the TPD spectra of the CH_4 + H + $^{18}O_2$ reaction (bottom)

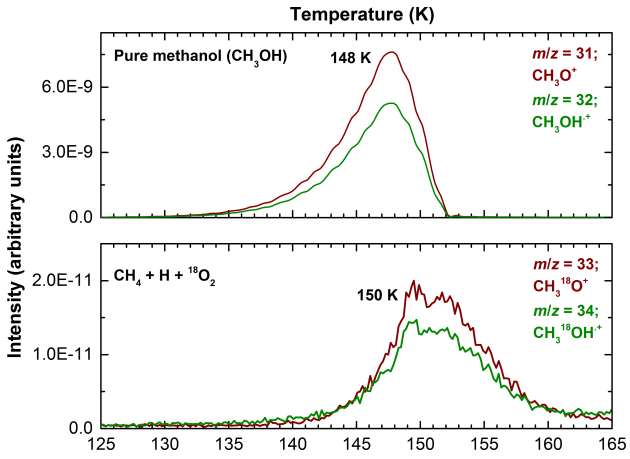

Fig. 1. TPD of pure CH_3OH (*top*; exp. 3.0) and TPD of the $CH_4 + H + {}^{18}O_2$ reaction (*bottom*; exp. 2.2).

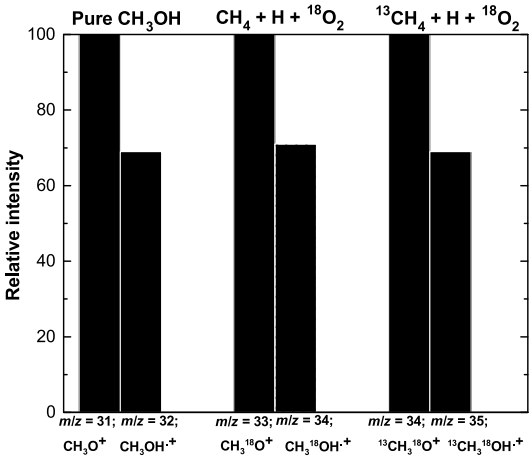

Fig. 2. Integrated QMS signals normalized to the integrated QMS signals of the $CH_3O^{\cdot+}$, $CH_3{}^{18}O^{\cdot+}$, and $^{13}CH_3{}^{18}O^{\cdot+}$ ions from the CH_3OH (exp. 3.0), $CH_4 + H + {}^{18}O_2$ (exp. 2.2), and $^{13}CH_4 + H + {}^{18}O_2$ (exp. 2.3) experiments, respectively. Ratios of the integrated intensities between the isotopes are in agreement with each other and with NIST values representing CH_3OH.

for m/z = 31, 32 and 33, 34, respectively. We note that m/z = 32 also represents the $O_2{}^{\cdot+}$ ion in the $CH_4 + H + O_2$ reaction, and therefore TPD data from the $^{18}O_2$ isotope experiment are used instead. Because m/z = 31 (CH_3O^+) and 32 ($CH_3OH^{\cdot+}$) represent the most intense ions for the CH_3OH cracking pattern found in our experimental setup and because their isotopically-induced shifted m/z values in the isotope-enriched experiments can be tracked for most experiments (i.e., the m/z values remain characteristic of CH_3OH and not of other species), we use the m/z values representing CH_3O^+ and $CH_3OH^{\cdot+}$ to confirm the formation of CH_3OH. As seen in Fig. 1 (top), the signals for m/z = 31 and 32 peak at 148 K for pure CH_3OH. The same m/z signals peak at 150 K in the $CH_4 + H + {}^{18}O_2$ experiment, as seen in Fig. 1 (bottom). This slight increase in the CH_3OH desorption temperature is expected since the binding energy of CH_3OH will be influenced by the presence of H_2O. It should be noted that H_2O, along with H_2O_2, are formed during the experiments and are not initial reactants of the ice mixture. The similar peak positions and profiles for the CH_3O^+ ($CH_3{}^{18}O^+$) and $CH_3OH^{\cdot+}$ ($CH_3{}^{18}OH^{\cdot+}$) ion signals between the two experiments allows to assign the observed desorption as originating from CH_3OH.

This assignment is further constrained by quantitatively comparing the CH_3OH fragmentation pattern upon 70 eV electron impact ionization with values available from the NIST database[1]. Figure 2 presents a column chart of the relative integrated intensities of the CH_3O^+ and $CH_3OH^{\cdot+}$ ion signals observed in a pure CH_3OH experiment and in isotopically-enriched $^{13}CH_4 + H + {}^{18}O_2$ experiments. As seen in Fig. 2, the relative integrated intensities of pure CH_3OH for m/z = 31 (CH_3O^+) and 32 ($CH_3OH^{\cdot+}$) are 100 and 69, respectively. In the $CH_4 + H + {}^{18}O_2$ experiment, the intensities for m/z = 33 ($CH_3{}^{18}O^+$) and 34 ($CH_3{}^{18}OH^{\cdot+}$) are 100 and 71, respectively. In the $^{13}CH_4 + H + {}^{18}O_2$ experiment, the values for m/z = 34 ($^{13}CH_3{}^{18}O^+$) and 35 ($^{13}CH_3{}^{18}OH^{\cdot+}$) are 100 and 69, respectively. In the NIST database, the relative integrated intensities for m/z = 31 (CH_3O^+) and 32 ($CH_3OH^{\cdot+}$) are 100 and 74, respectively. The relative integrated intensities in the three experiments are nearly identical and are close to the values from NIST, fully in line with CH_3OH formation in the ice.

[1] NIST Mass Spec Data Center, S. E. Stein, director, "Mass Spectra" in NIST Chemistry WebBook, NIST Standard Reference Database Number 69, Eds. P. J. Linstrom and W. G. Mallard, National Institute of Standards and Technology, Gaithersburg MD, 20899, doi: 10.18434/T4D303, (retrieved November 7, 2017).

3.1.2. RAIRS

Figure 3 shows the resulting 4000–700 cm^{-1} (2.5–14.3 μm) spectrum for $CH_4 + H + O_2$ interacting on a 10 K substrate. Table 2 lists the frequencies measured, as well as the identification of species observed and the corresponding vibrational modes. The assignment of the peaks are constrained by considering literature values, isotope experiments, ice desorption temperatures, and varying flux ratios of the reactants. The inset in Fig. 3 shows a band at 1001 cm^{-1} that is assigned to the C–O stretching mode of CH_3OH. This assignment is based on experiments performed in Sect. 3.2. Literature values for this band (Wada et al. 2006; Hodyss et al. 2009; Martín-Doménech et al. 2016) are normally somewhat higher; around 1015 cm^{-1} when CH_3OH is mixed with H_2O. Even though this band is rather weak, it offers a tool to unambiguously link to CH_3OH as it has no overlap with bands of other species formed in these experiments and actually provides a nicely isolated feature.

A series of additional experiments are performed in order to further prove that the band at 1001 cm^{-1} is indeed due to the C–O stretching frequency of CH_3OH. This is realized in a set of isotope substitution experiments. Figure 4 shows spectra of three experiments that involve CH_4, $^{13}CH_4$, O_2, and $^{18}O_2$ isotopes. By the simple harmonic oscillator approach, a heavier isotope should result in a redshift in the stretching frequency. As seen in Fig. 4, the 1001 cm^{-1} feature redshifts to 984 cm^{-1} and 973 cm^{-1} for the reactions involving $^{13}CH_4$ and $^{18}O_2$, respectively. This leads to differences of 17 cm^{-1} and 28 cm^{-1} from the 1001 cm^{-1} feature, respectively, comparable to the differences found in CH_3OH isotope experiments performed by Maity et al. (2014). These findings are consistent with isotopically enriched C–O bonds in newly formed CH_3OH.

3.1.3. Temperature-dependent RAIR difference spectra

The TPD and RAIRS data can be correlated to one another to match IR features with desorption temperatures to further identify species that are initially made in the ice (i.e., before thermal processing via the TPD technique). Figure 5 shows the change in the IR features as a function of the substrate temperature (i.e., RAIR difference spectra) for the $CH_4 + H +$

Table 2. Infrared ice signatures from the CH_4 + H + O_2 reaction and the corresponding vibrational modes.

Peak position (cm^{-1})	Peak position (μm)	Molecule	Mode*	Reference
884	11.3	H_2O_2	υ_3	1, 2, 3
1001	9.99	CH_3OH	υ_8	this work
1302	7.68	CH_4	υ_4	4, 5, 7, 8, 9
1381	7.24	H_2O_2	υ_2	1, 2, 3
1637	6.11	H_2O	υ_2	6
2815	3.55	CH_4	$\upsilon_2 + \upsilon_4$	4, 5, 7, 8, 9
2836	3.53	H_2O_2	$2\upsilon_2$	1, 2, 3
2902	3.45	CH_4	υ_1	7, 8, 9
3010	3.32	CH_4	υ_3	4, 5, 7, 8, 9
3295	3.0	H_2O_2 + H_2O	O–H stretch	10, 11
3675	2.7	H_2O	dangling bonds	7

Notes. (*) The vibrational mode numbers are obtained from NIST.
References [1] Giguere & Harvey (1959), [2] Lannon et al. (1971), [3] Romanzin et al. (2011), [4] Hagen et al. (1981), [5] Gerakines et al. (2005), [6] Hodyss et al. (2009), [7] Gálvez et al. (2009), [8] Herrero et al. (2010), [9] Ennis et al. (2011), [10] Cuppen et al. (2010), [11] Ioppolo et al. (2010).

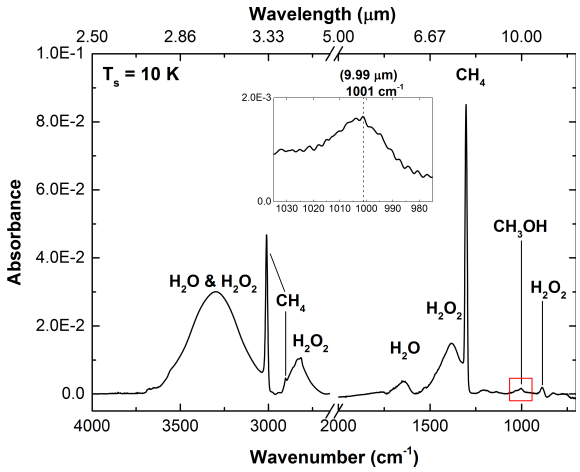

Fig. 3. RAIR spectrum of the reaction, CH_4 + H + O_2, on a 10 K substrate surface after 12 hours (exp. 1.0). The relative column density of CH_4:CH_3OH is 100:1, and the relative column density of H_2O:CH_3OH is 100:4. Spectra of the resulting species are shown (see Table 2), most noticeably a weaker band around 1000 cm^{-1} (inset) highlighting the C–O stretch of the CH_3OH feature.

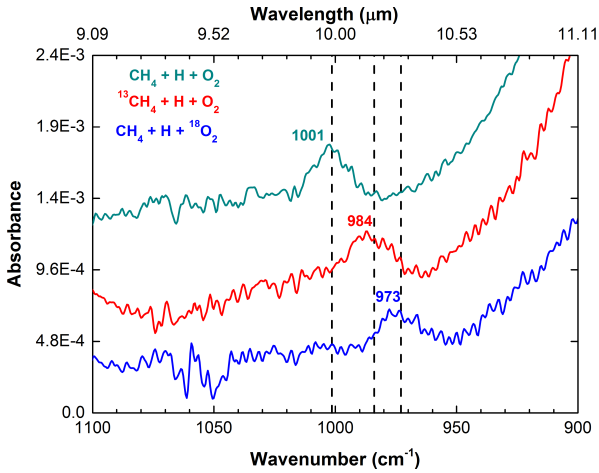

Fig. 4. RAIR spectra of the reactions, CH_4 + H + O_2 (exp. 2.0), $^{13}CH_4$ + H + O_2 (exp. 2.1), and CH_4 + H + $^{18}O_2$ (exp. 2.2) on a 10 K substrate surface after 6 hours each.

O_2 reaction. In Sect. 3.1.1 the desorption of CH_3OH is observed at 150 K, and in Sect. 3.1.2 the IR feature at 1001 cm^{-1} is shown to be due to CH_3OH formation. The combination of these two pieces of data tells us that below 150 K, CH_3OH should be present in the ice, and above 150 K a majority of the CH_3OH should desorb. In Fig. 5, the C–O bond feature remains present at a substrate temperature of 145 K and is absent at a substrate temperature of 155 K. This correlates well with the desorption temperature of CH_3OH observed in Fig. 1 (bottom). Thus, the experiments discussed in Sects. 3.1.1–3.1.3 make a consistent case that CH_3OH is formed in the ice.

3.2. Spectral signature of CH_3OH in a H_2O-rich interstellar ice analogue

Because the C–O bond of CH_3OH is known to be sensitive to its surrounding environment, it holds a potential as a diagnostic tool to provide a deeper insight to the interactions of CH_3OH with

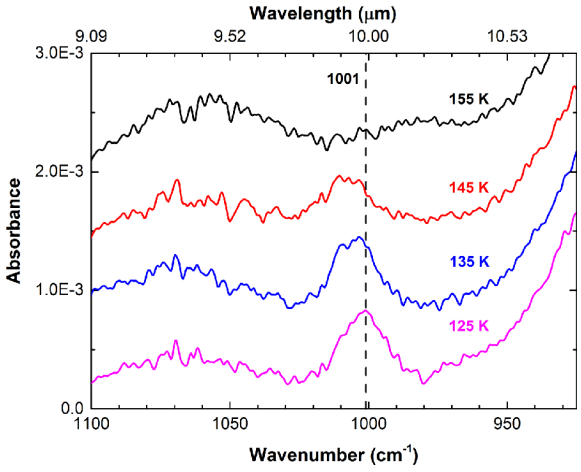

Fig. 5. RAIR difference spectra of the CH_4 + H + O_2 reaction (exp. 2.0). The 1001 cm^{-1} feature blueshifts between 125 K and 145 K, and could be due to CH_3OH segregating in a H_2O–ice environment (Martín-Doménech et al. 2014), and disappears upon further heating to 155 K.

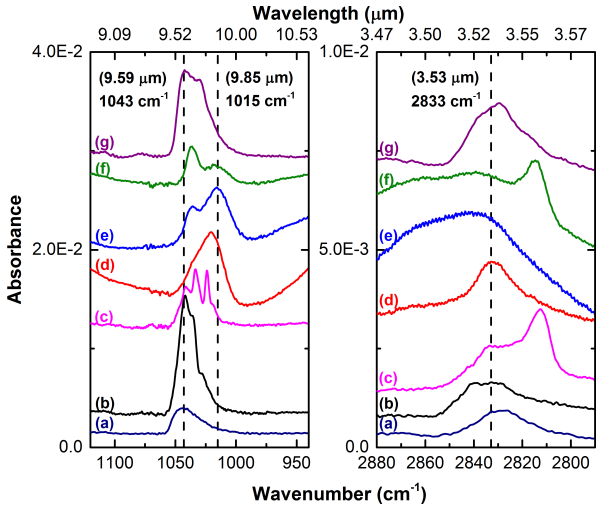

Fig. 6. *Left*: RAIR spectra of the C–O stretch of CH_3OH when CH_3OH is mixed with different species. (*a*) Pure CH_3OH (exp. 4.0), (*b*) CH_3OH + O_2 (exp. 4.1), (*c*) CH_3OH + CH_4 (exp. 4.2), (*d*) CH_3OH + H_2O (exp. 4.3), (*e*) CH_3OH + H_2O (exp 4.4), (*f*) CH_3OH + H_2O + CH_4 (exp 4.5), and (*g*) CH_3OH + CO (exp 4.6). *Right*: RAIR spectra of the symmetric C–H stretch of CH_3OH.

other species in the H_2O-rich interstellar ice analogue. Figure 6 (left) shows a RAIR spectrum of the C–O stretching frequency of pure CH_3OH (a) in comparison to CH_3OH embedded in an environment originating from the CH_4 + H + O_2 reaction (f), in addition to CH_3OH mixed with other species (b–e, g). Figure 6 (right) shows a RAIR spectrum of the C–H stretch of pure CH_3OH; a mode that is a useful tracer of CH_3OH ice and can be probed by observational facilities (e.g., JWST NIRSpec). The experiments are performed using both the previously described HABS and a microwave atom source (MWAS), which dissociates a fraction of the incoming molecules into fragments. The fragments can recombine with each other and form products in the ice that would be found in, for example, the CH_4 + H + O_2 reaction (OH, H, O_2, O, H_2, H_2O_2, etc.). The C–O stretching frequency of pure CH_3OH is found at 1043 cm^{-1} and redshifts to 1015 cm^{-1} in the ice where CH_4 and fragments from dissociated H_2O are co-deposited. We note that the peak does not redshift to 1001 cm^{-1}, and there is a logical explanation for this. As illustrated in Fig. 7 in the study by Dawes et al. (2016), an increase in the H_2O concentration in a CH_3OH + H_2O mixture does not necessarily correlate to a more redshifted C–O stretching frequency. Thus, it is expected that a specific ratio of the ice products in the CH_4 + H + O_2 reaction is needed in order to recreate the 1001 cm^{-1} feature. From the spectra presented in Fig. 6, it is clear that the largest redshift for the C–O stretch takes place in a H_2O-rich ice matrix that contains CH_4, H_2O, and H_2O dissociation products (i.e., the mixture in the actual CH_4 + H + O_2 experiment; exp. 4.5), as expected. When CH_3OH is mixed with a single species, such as H_2O or CH_4, the C–O stretching frequency does not redshift as much. In conclusion, it is proposed that many, rather than one or two molecular species, interact simultaneously with CH_3OH in the CH_4 + H + O_2 reaction.

3.3. CH_3OH formation at 10 and 20 K

As mentioned in Sect. 2, an absolute value for the CH_3OH column density is not obtained in this study. Thus, in order to provide information on the formation yield of CH_3OH formed at 10–20 K, a relative yield is obtained by comparing the amount of CH_3OH formed at 10 K (exp. 2.0) to the amount of CH_3OH formed at 20 K (exp. 5.0). Since it is expected in interstellar space that CH_4 and H_2O ice are initially formed by hydrogenation reactions (Tielens & Hagen 1982; Öberg et al. 2008; Ioppolo et al. 2008; Cuppen et al. 2010; van Dishoeck et al. 2013), the CH_4:H_2O ice ratio should not be drastically different between surface temperatures of 10 and 20 K. Therefore, the CH_4:H_2O ice ratio is kept the same in this temperature range. At 20 K, a 65% decrease in the CH_3OH abundance is observed compared to the amount of CH_3OH formed at10 K. This decrease in abundance is expected to be due to the decrease in the H-atom lifetime on the surface (Fuchs et al. 2009; Cuppen et al. 2010), as expected if CH_3OH is being formed by the OH radical. Although, it should be noted that the reaction steps for CH_3OH formation may also be affected by the temperature change, which can influence the change in the CH_3OH abundance.

3.4. Constraining the formation of CH_3OH in the overall reaction network

The experiments discussed here show that it is possible to form CH_3OH in a H_2O-rich environment along the low temperature pathway:

$$CH_4 + OH \rightarrow CH_3 + H_2O \quad (1a)$$

$$CH_3 + OH \rightarrow CH_3OH \quad (1b)$$

To observe how these channels fit into the overall reaction network ongoing in H_2O-rich ice, the change in abundances of CH_3OH and other ice species needs to be tracked (Öberg et al. 2010). Figure 7 shows two RAIR spectra of the reaction, CH_4 + H + O_2, and the subsequent infrared features pertaining to newly formed CH_3OH, H_2O, H_2O_2, and O_3. With an enhancement of the O_2 flux (dashed line in Fig. 7), the CH_3OH abundance decreases and the H_2O_2 and O_3 abundances clearly increase. The decrease in the CH_3OH abundance at the expense of the H_2O_2 and O_3 abundances gives an indication that the formation channel of CH_3OH at least crosses with the formation channels of H_2O_2 and O_3.

The link between the formation of CH_3OH, H_2O_2, and O_3 in the H_2O-rich ice can be better understood when looking at the reaction network presented by Cuppen et al. (2010). In this study, the H + O_2 reaction is extensively discussed, and it is found that the O atom used to react with O_2 to form O_3 is most likely created by two reactions,

$$H + HO_2 \rightarrow H_2O + O \quad (2)$$

and

$$OH + O_2 \rightarrow HO_2 + O \quad (3a)$$

where OH is mainly formed by the following reaction:

$$H + HO_2 \rightarrow 2OH \quad (3b)$$

We note that only the relevant steps are discussed here, and the full reaction scheme can be found in Cuppen et al. (2010). The RAIR spectra shown in Fig. 7 suggest that the latter reactions are dominant in the CH_4 + H + O_2 reaction. As observed in Fig. 7, a threefold increase in the O_2 flux (exp. 2.0 has a threefold increase in the O_2 flux compared to exp. 6.0) results in a substantial increase in the H_2O_2 abundance compared to the change in the H_2O abundance. This is consistent with reactions (3a) and (3b) as HO_2 is an intermediate of the

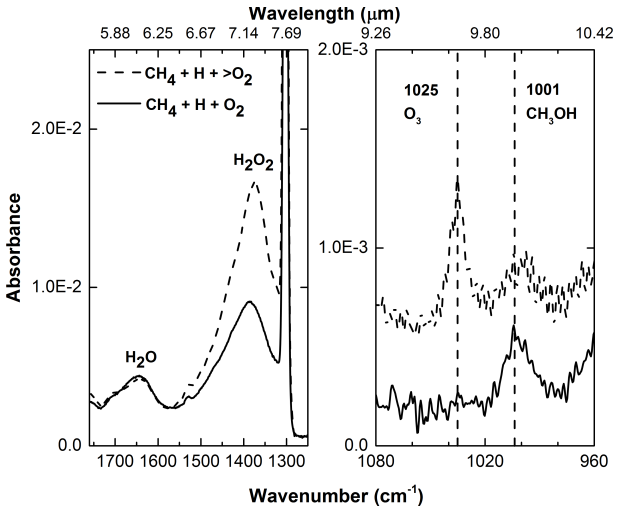

Fig. 7. RAIR spectra of the reactions, CH_4 + H + O_2, where >O_2 indicates a threefold increase in the O_2 flux. The dashed–line spectrum corresponds to exp. 2.0, and the solid–line spectrum corresponds to exp. 6.0.

H_2O_2 product; HO_2 is also an intermediate of H_2O formation, as shown in reaction (2). However, comparison of the two spectra in Fig. 7 shows that an increase in the O_3 abundance is followed by a significant difference in the H_2O_2 abundance and a relatively minor change in the H_2O abundance, suggesting that reactions (3a) and (3b) are carried out more efficiently than reaction (2) in the CH_4 + H + O_2 experiment. Decreasing the CH_4 abundance by 20% shows a 10% decrease in the CH_3OH abundance and no change in the H_2O abundance, which further supports that reaction (2) is not the dominating channel. In addition, reactions (3a) and (3b) show that O_3 is formed by an OH-induced process, and this is expected since CH_3OH is formed by an OH-mediated reaction. These insights piece together to demonstrate that reactions (3a) and (3b) are the likely pathways that connect the formation channel of CH_3OH to other formation channels in a H_2O-rich ice reaction network. In Fig. 8, the laboratory experiments and the astrochemical proposed reactions are summarized in one figure. The main difference between the two is how OH radicals are inserted into the reaction scheme, but this does not change the conclusions derived here for the presented pre-CO freeze-out formation scheme.

4. Astrophysical implications

The experimental work presented here calls into question the A_V at which CH_3OH ice starts to grow (i.e., the CH_3OH ice formation threshold). If an observational search for the CH_3OH ice formation threshold in low extinction (i.e., H_2O-rich) environments is to be performed, it would be useful to know beforehand an approximation of the CH_3OH abundance in these H_2O-rich ices. That way, the amount of CH_3OH formed before and after the CO freeze-out stage can be distinguished. A laboratory experiment of CO + H performed under similar conditions to exp. 2.0 shows that the CO:CH_3OH ratio is 100:20. In the parallel CH_4 + OH experiment, the CH_4:CH_3OH ratio is 100:1. A comparison of these two experiments leads to the conclusion that the CH_4 + OH reaction is 20 times less efficient at producing CH_3OH than the CO + H reaction in the laboratory setting. Making the simple assumption that CH_3OH is primarily formed by CH_4 + OH and CO + H in interstellar ices around the CO freeze–out stage, laboratory data can be combined with

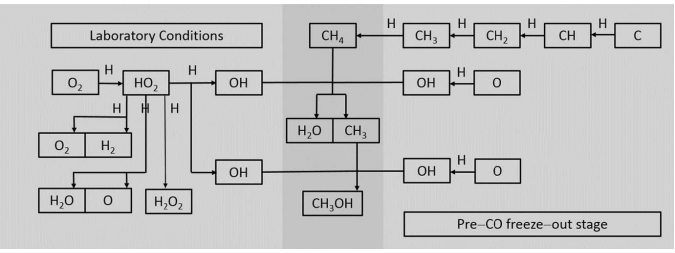

Fig. 8. Comparison of the laboratory work discussed here and the astrochemical network, resulting in the formation of CH_3OH in the pre-CO freeze-out stage. Only the relevant steps are shown.

observational data to determine the amount of CH_3OH in the two different ice phases. According to Boogert et al. (2015), the H_2O:CH_4 and H_2O:CO median ice ratios around low mass young stellar objects (LYSOs) are 100:4.5 and 100:21, respectively. Incorporation of the laboratory results shows that 0.045% of the interstellar ice should contain CH_3OH that derives from CH_4, and 4.2% of the ice should contain CH_3OH that derives from CO. Thus, of the total observed abundance of CH_3OH, about 1% of the total amount is the abundance of CH_3OH from the CH_4 + OH reaction that is expected to be ongoing in the H_2O-rich ice phase. Although a CH_3OH:H_2O percentage of 0.045% may appear insignificant, multiplying this value by the typical H_2O ice to H ratio of 2E–5 yields a CH_3OH ice to H ratio of 9E–9, which is greater than the abundance of gas-phase CH_3OH and other gas-phase species detected in cold cores relative to H_2 (Herbst & Van Dishoeck 2009). Using values from the 20 K experiment (exp. 5.0), the CH_3OH ice to H ratio results in a value of 3E–9, which is similar to the abundance of gas-phase CH_3OH in these particular astrophysical environments. We note that the median ice ratios contain sources that also have a relatively high amount of CO ice, so the calculated values are not entirely representative of low extinction (i.e., H_2O-rich ice) scenarios. See Fig. 9 for a better approximation of the possible CH_3OH abundance in the H_2O-rich ice layer at various extinctions.

Figure 9, which is adapted from Boogert et al. (2015), shows that CH_3OH detections have an ice formation threshold at an A_V value higher than H_2O and CO (the ice formation threshold in this figure is the X-axis cut-off divided by 2 because the background stars trace both the front and back sides of the clouds). This is in line with the currently accepted model that CH_3OH ice is mainly formed in prestellar cores at $A_V > 9$ via hydrogenation of accreted CO molecules. However, what is puzzling is that the upper limit sight lines are all below the detections and at similar A_V values to that of the detections. The CH_3OH:H_2O ratio of 4:100 derived from the laboratory work presented here (from exp. 1.0) is represented by the dashed blue line and is at the level of 3-σ upper limits. Thus, the current observations are consistent with a CH_3OH:H_2O ratio of at most a few percent, though likely not as high as 4%, the value seen in our optimized experiments, since H_2O is a by-product in the CH_4 + H + O_2 reaction and is not the main source of H_2O in interstellar ices. At this level, a formation threshold as low as that of H_2O (1.6 mag) as a result of chemical reactions in H_2O-rich ices cannot be excluded. More sensitive observations are needed to further constrain this scenario and with the upcoming launch of the JWST, this soon will be within range.

The insights gained here also link to the formation of larger COMs. Reaction (1) gives rise to the possibility that such a mechanism could lead to the formation of more complex species in H_2O-rich ices. It has been shown that COMs such as

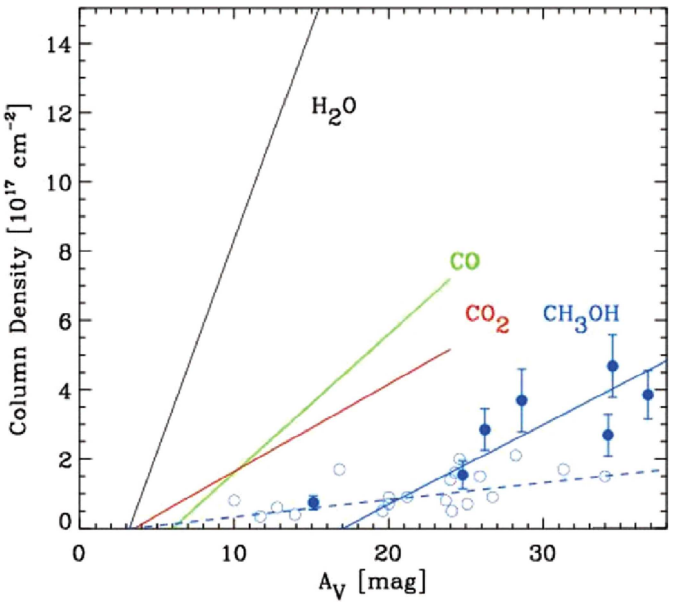

Fig. 9. Relationships between ice column density and visual extinction (A_V) as observed toward stars behind dense clouds and cores for H_2O (black), CO (green), CO_2 (red), and CH_3OH (blue). For clarity, for H_2O, CO, and CO_2, the least-squares linear fits are shown and not the actual data points. For CH_3OH, blue bullets indicate detections with 1-σ error bars and open circles indicate 3-σ upper limits. The solid blue line is a fit to the detections, and the dashed blue line (from exp. 1.0) indicates the scenario in which CH_3OH has the same ice formation threshold as H_2O at a maximum abundance of CH_3OH:H_2O = 4%, as found in the listed experiments. The 3 σ upper limits prove in principle that CH_3OH:H_2O is less than 4% in the observed sight lines. This figure was adapted from Fig. 7 in Boogert et al. (2015).

glycolaldehyde, ethylene glycol, and glycerol can be successfully formed by hydrogenation of CO (Fedoseev et al. 2015, 2017), thus providing a promising reaction scheme for COM formation in CO-rich interstellar ices. Formation of COMs in H_2O-rich ices has been less studied, and the mechanism described in this paper could be a potential source of molecular complexity in cold H_2O-dominated ice matrices, although formation efficiencies will be lower.

5. Conclusions

The formation of CH_3OH by CH_4 + OH shown in this laboratory study suggests that CH_3OH ice can also be formed before the heavy CO freeze-out stage in prestellar cores, i.e., at $A_V < 3$ and grain temperatures of 20 K. The main findings from this work are summarized below:

- The formation of CH_3OH in H_2O-rich ices occurs by the sequential reactions, $CH_4 + OH \rightarrow CH_3 + H_2O$ and $CH_3 + OH \rightarrow CH_3OH$.
- Since CH_4 and OH radicals are expected to be found in the H_2O-rich ice phase of cold dense cores, CH_3OH is also expected to be found in those ices, suggesting that the CH_3OH formation threshold is below $A_V = 9$.
- Raising the sample temperature to 20 K results in a 65% decrease in the CH_3OH abundance compared to CH_3OH formed on a 10 K surface, showing that the formation pathway of CH_3OH in this study is relevant to the period of the cold dense core stage at which ice species are formed primarily by atom-induced reactions (i.e., before gas phase molecules, like CO, accrete onto the grain surface).
- Under similar experimental parameters, the CO + H channel is about 20 times more efficient to forming CH_3OH than the CH_4 + OH channel at temperatures around 10 K.
- More sensitive astronomical observations are warranted to determine the CH_3OH:H_2O ratio in H_2O-rich interstellar ices, which is likely to be a few percent at most, as derived from Fig. 9.
- The formation of COMs under cold dark cloud conditions is mainly linked to the CO freeze-out stage. The reactions studied here carry the potential to lead to the formation of COMs at an earlier astrochemical evolution stage.

Acknowledgements. This research was funded by the Dutch Astrochemistry Network II (DANII), through a VICI grant of NWO (the Netherlands Organization for Scientific Research), and A-ERC grant 291141 CHEMPLAN. The financial support by NOVA (the Netherlands Research School for Astronomy) and the Royal Netherlands Academy of Arts and Sciences (KNAW) through a professor prize is acknowledged. G. F. acknowledges the financial support from the European Union's Horizon 2020 research and innovation programme under the Marie Sklodowska-Curie grant agreement n. 664931. S.I. acknowledges the Royal Society for financial support and the Holland Research School for Molecular Chemistry (HRSMC) for a travel grant. D.Q. is thankful to Daniel Harsono, Ewine van Dishoeck, Thanja Lamberts, and Vianney Taquet for enlightening discussions leading to this publication.

References

Allamandola, L., Sandford, S., Tielens, A., et al. 1992, ApJ, 399, 134
Bergman, P., Parise, B., Liseau, R., & Larsson, B. 2011, A&A, 527, A39
Bergner, J. B., Öberg, K. I., & Rajappan, M. 2017, ApJ, 845, 29
Boogert, A. C. A., Schutte, W., Helmich, F., et al. 1997, A&A, 317, 929
Boogert, A. C. A., Pontoppidan, K. M., Knez, C., et al. 2008, ApJ, 678, 985
Boogert, A. C. A., Huard, T., Cook, A., et al. 2011, ApJ, 729, 92
Boogert, A. C. A., Gerakines, P. A., & Whittet, D. C. 2015, ARA&A, 53, 541
Bossa, J.-B., Paardekooper, D., Isokoski, K., & Linnartz, H. 2015, Phys. Chem. Chem. Phys., 17, 17346
Bottinelli, S., Boogert, A. A., Bouwman, J., et al. 2010, ApJ, 718, 1100
Bouilloud, M., Fray, N., Bénilan, Y., et al. 2015, MNRAS, 451, 2145
Chiar, J., Adamson, A., & Whittet, D. 1996, ApJ, 472, 665
Chuang, K.-J., Fedoseev, G., Ioppolo, S., et al. 2015, MNRAS, 455, 1702
Chuang, K.-J., Fedoseev, G., Qasim, D., et al. 2017, MNRAS, 467, 2552
Cuppen, H., & Herbst, E. 2007, ApJ, 668, 294
Cuppen, H., van Dishoeck, E., Herbst, E., et al. 2009, A&A, 508, 275
Cuppen, H., Ioppolo, S., Romanzin, C., et al. 2010, Phys. Chem. Chem. Phys., 12, 12077
Cuppen, H., Penteado, E., Isokoski, K., et al. 2011, MNRAS, 417, 2809
Dartois, E., Schutte, W., Geballe, T., et al. 1999, A&A, 342, L32
Dawes, A., Mason, N. J., & Fraser, H. J. 2016, Phys. Chem. Chem. Phys., 18, 1245
d'Hendecourt, L., Jourdain de Muizon, M., Dartois, E., et al. 1996, A&A, 315, L365
Ennis, C., Yuan, H., Sibener, S., et al. 2011, Phys. Chem. Chem. Phys., 13, 17870
Fedoseev, G., Cuppen, H. M., Ioppolo, S., et al. 2015, MNRAS, 448, 1288
Fedoseev, G., Chuang, K., Ioppolo, S., et al. 2017, ApJ, 842, 9
Friberg, P., Hjalmarson, A., Madden, S., et al. 1988, A&A, 195, 281
Fuchs, G., Cuppen, H., Ioppolo, S., et al. 2009, A&A, 505, 629
Gálvez, Ó., Maté, B., Herrero, V. J., et al. 2009, ApJ, 703, 2101
Garrod, R., Park, I. H., Caselli, P., et al. 2006, Faraday Discuss., 133, 51
Geppert, W. D., Hamberg, M., Thomas, R. D., et al. 2006, Faraday Discuss., 133, 177
Gerakines, P. A., Bray, J., Davis, A., et al. 2005, ApJ, 620, 1140
Gibb, E., Whittet, D., Schutte, W. a., et al. 2000, ApJ, 536, 347
Gibb, E., Whittet, D., Boogert, A., & Tielens, A. 2004, ApJS, 151, 35
Giguere, P., & Harvey, K. 1959, J. Mol. Spectr., 3, 36
Grim, R., Baas, F., Greenberg, J., et al. 1991, A&A, 243, 473
Guzmán, V., Goicoechea, J., Pety, J., et al. 2013, A&A, 560, A73
Hagen, W., Tielens, A., & Greenberg, J. 1981, J. Chem. Phys., 56, 367
Herbst, E., & Van Dishoeck E. F. 2009, ARA&A, 47, 427
Herrero, V. J., Gálvez, Ó., Maté, B., et al. 2010, Phys. Chem. Chem. Phys., 12, 3164
Hiraoka, K., Ohashi, N., Kihara, Y., et al. 1994, Chem. Phys. Lett., 229, 408
Hodyss, R., Johnson, P. V., Stern, J. V., et al. 2009, Icarus, 200, 338
Hudgins, D., Sandford, S., Allamandola, L., et al. 1993, ApJS, 86, 713
Ioppolo, S., Cuppen, H., Romanzin, C., et al. 2008, ApJ, 686, 1474

Ioppolo, S., Cuppen, H., Romanzin, C., et al. 2010, Phys. Chem. Chem. Phys., 12, 12065
Ioppolo, S., Fedoseev, G., Lamberts, T., et al. 2013, Rev. Sci. Instrum., 84, 073112
Kolasinski, K. W. 2012, Surface Science: Foundations of Catalysis and Nanoscience (John Wiley & Sons)
Lamberts, T., Cuppen, H. M., Ioppolo, S., et al. 2013, Phys. Chem. Chem. Phys., 15, 8287
Lamberts, T., Fedoseev, G., Kästner, J., et al. 2017, A&A, 599, A132
Lannon, J. A., Verderame, F. D., & Anderson Jr R. W. 1971, J. Chem. Phys., 54, 2212
Linnartz, H., Ioppolo, S., & Fedoseev, G. 2015, Int. Rev. Phys. Chem., 34, 205
Loeffler, M., Raut, U., Vidal, R., et al. 2006, Icarus, 180, 265
Maity, S., Kaiser, R. I., & Jones, B. M. 2014, Faraday Discuss., 168, 485
Martín-Doménech, R., Caro, G. M., Bueno, J., & Goesmann, F. 2014, A&A, 564, A8
Martín-Doménech, R., Caro, G. M., & Cruz-Díaz, G. 2016, A&A, 589, A107
Moore, M., & Hudson, R. 1998, Icarus, 135, 518
Oba, Y., Watanabe, N., Hama, T., et al. 2012, ApJ, 749, 67
Öberg, K. I., Boogert, A. A., Pontoppidan, K. M., et al. 2008, ApJ, 678, 1032
Öberg, K. I., Garrod, R. T., van Dishoeck, E. F., et al. 2009, A&A, 504, 891
Öberg, K. I., van Dishoeck, E. F., Linnartz, H., & Andersson, S. 2010, ApJ, 718, 832
Öberg, K. I., Boogert, A. A., Pontoppidan, K. M., et al. 2011, ApJ, 740, 109
Öberg, K. I., Fayolle, E. C., Reiter, J. B., & Cyganowski, C. 2014, Faraday Discuss., 168, 81
Paardekooper, D., Fedoseev, G., Riedo, A., et al. 2016, A&A, 596, A72
Parise, B., Ceccarelli, C., Tielens, A., et al. 2002, A&A, 393, L49
Penteado, E., Boogert, A., Pontoppidan, K., et al. 2015, MNRAS, 454, 531
Pontoppidan, K. M. 2006, A&A, 453, L47
Pontoppidan, K. M., Dartois, E., van Dishoeck, E. F., Thi, W.-F., & d'Hendecourt, L. 2003, A&A, 404, L17
Romanzin, C., Ioppolo, S., Cuppen, H., et al. 2011, J. Chem. Phys., 134, 084504
Schutte, W. A. 1988, Ph.D. Thesis (Leiden: Rijksuniversiteit)
Skinner, C., Tielens, A., Barlow, M., et al. 1992, ApJ, 399, L79
Taban, I., Schutte, W., Pontoppidan, K., et al. 2003, A&A, 399, 169
Taquet, V., López-Sepulcre, A., Ceccarelli, C., et al. 2015, ApJ, 804, 81
Teolis, B., Loeffler, M., Raut, U., et al. 2007, Icarus, 190, 274
Tielens, A., & Hagen, W. 1982, A&A, 114, 245
Tschersich, K. 2000, J. Appl. Phys., 87, 2565
Tschersich, K., & Von Bonin V. 1998, J. Appl. Phys., 84, 4065
Tschersich, K., Fleischhauer, J., & Schuler, H. 2008, J. Appl. Phys., 104, 034908
Turner, B. 1998, ApJ, 501, 731
van Dishoeck, E. F. 1998, The Chemistry of Diffuse and Dark Interstellar Clouds (Oxford: Oxford University Press)
van Dishoeck, E. F. 2017, ArXiv e-prints [arXiv: 1710.05940]
van Dishoeck, E. F., Herbst, E., & Neufeld, D. A. 2013, Chem. Rev., 113, 9043
Vandenbussche, B., Ehrenfreund, P., Boogert, A., et al. 1999, A&A, 346, L57
Wada, A., Mochizuki, N., & Hiraoka, K. 2006, ApJ, 644, 300
Watanabe, N., & Kouchi, A. 2002, ApJ, 571, L173
Weber, A. S., Hodyss, R., Johnson, P. V., et al. 2009, ApJ, 703, 1030
Wirström, E., Geppert, W. D., Hjalmarson, Å., et al. 2011, A&A, 533, A24
Zins, E.-L., Pirim, C., Joshi, P. R., et al. 2012, J. Phys. Chem. A, 116, 12357